

# AO:08 Two Independent Studies of Atmospheric Aerosols. I: Hygroscopic Growth & II: Aircraft Emissions

Supervisors: Dr R D Grainger & Dr D Peters  
Candidate No.: 44824  
Word Count: 6 561

## 1 Abstract

Originally, the investigation was focused on the nature of hygroscopic growth in atmospheric aerosols, with the initial time spent researching current literature on the subject. Prior to the start of experimental work on hygroscopic growth, an opportunity arose for fieldwork relating to the emission of particulate matter from aircraft. Subsequently, the direction of the project was altered to facilitate involvement in the important research area of aviation emissions. Both aspects of the investigation are included due to the significant time spent on each subject.

The experimental setup for an investigation into the hygroscopic growth of ammonium nitrate and ammonium sulphate aerosols is proposed, with reference to future study of the optical properties of atmospheric aerosols. The proposed setup uses an ultrasonic nebuliser and diffusion dryer to produce a quasi-monodisperse aerosol which undergoes humidification in a conditioner of variable  $RH$  (0% - 100%) prior to being measured by an optical particle counter.

Following recent EU directives to limit  $PM_{2.5}$  and  $PM_{10}$  emissions due to their health risks, the second part of the report details the study of aircraft particulate emissions from a BAE-146 on 17/02/2009 at Cranfield airport, Bedfordshire. The experiment used an optical particle counter (OPC) and condensation particle counter (CPC) with the intention of obtaining a size distribution of tyre emissions. SPARCLE, a recently developed advanced optical particle counter, was also deployed for the first time to act as a field test. There was no evidence of emissions from the OPC or SPARCLE data, however the CPC detected aerosol plumes of concentration between  $1 \times 10^5 \text{ cm}^{-3}$  and  $8 \times 10^5 \text{ cm}^{-3}$  during taxi, take-off and landing; above an ambient aerosol of  $5 \times 10^3 \text{ cm}^{-3}$ . These plumes were attributed to engine emissions due to the observed smell of kerosene.

The size distribution of a sample of tyre and brake

emission brushings from the undercarriage of a BAE-146 was obtained using an aerosol disperser and sizer; 3 distinct peaks were evident for particulates with diameters of  $1.2 \mu\text{m}$ ,  $7.0 \mu\text{m}$  and  $35 \mu\text{m}$ . We find that  $\sim 0.1\%$  by mass is classed as  $PM_{10}$  with only  $\sim 10^{-4}\%$  in the  $PM_{2.5}$  category.

## 2 Introduction

An aerosol is defined as a suspension of particles in a gas [1]. Both aspects of this study relate to aerosols and their associated atmospheric and health effects.

Aerosols are an important atmospheric constituent; their perturbation on the radiative balance of the Earth's climate system is classified into direct and indirect effects. The direct effect is due to the scattering and absorption of short-wave solar and long-wave thermal radiation by the aerosol particulates. Key factors in determining whether a particular aerosol has a net positive (heating) or negative (cooling) direct radiative forcing influence on the Earth's radiation budget include the spatial distribution of the aerosol, its physical state and associated optical properties [2], which depend on the hygroscopicity of the aerosol [3]. Hygroscopy is the ability of a substance to attract water molecules from the ambient environment via absorption.

The indirect effect refers to aerosols altering the radiative properties, amount and lifetime of clouds through their role as cloud condensation nuclei (CCN) by primarily affecting the droplet number concentration and size. A higher concentration of aerosols causes an increased concentration of cloud droplets which enhances the cloud albedo, thus reducing the solar radiation which reaches the lower atmosphere and Earth's surface. Precipitation is also affected by the presence of aerosols; increased CCN concentration reduces the mean droplet size which lengthens the cloud lifetime and inhibits precipita-

tion [4].

Aerosols in the atmosphere are both natural and anthropogenic in origin. The principal natural aerosols are sea salt, produced by the interaction of the wind with the ocean surface and sulphate emissions from volcanoes and from marine phytoplankton [4]. The main anthropogenic particles are sulphates, black carbon from fossil fuel burning and mineral dust due to agricultural practices. The importance of the influence of aerosols on the Earth-atmosphere radiation budget has been highlighted in recent quantitative studies of the aerosol direct radiative effect (DRE), which is the sum of the direct effects due to anthropogenic and natural aerosols. These displayed a diurnally averaged global mean of  $-5.4 \text{ Wm}^{-2}$  with a standard deviation of  $0.9 \text{ Wm}^{-2}$  [9]. The same report states that the combined radiative forcing due to increases in the atmospheric content of carbon dioxide, methane and nitrous oxide (compared to pre-industrial 1750 values) is  $+2.30 \text{ Wm}^{-2}$ . The effects of increases in the concentrations of greenhouse gases have been widely publicised [10] [11] [12]; by comparison the contribution of greenhouse gases to radiative forcing is less than half that of aerosols. This emphasises the need to ensure continual research into aerosols and their associated climate mechanisms.

Besides the climatic influence of aerosols, there are also significant health effects associated with localised sources of anthropogenic particulate matter. The second area of study in this report examines particulate emissions at an airport with emphasis on the size distribution of tyre smoke. The World Health Organisation highlights the health effects of particulate matter in its most recent review [38] of air quality, stating that the long term effects include; a reduction in life expectancy due to an increase in pulmonary cancer, increases in respiratory symptoms, increases in chronic obstructive pulmonary disease and reduced lung function in children and adults. The ACRP [34] supports these findings adding further that fine and ultrafine aerosol particles have been linked to heart attacks, bronchitis and asthma.

The health effects of particulates is related to the site of deposition in the respiratory system. Coarse particles ( $1 \mu\text{m} - 10 \mu\text{m}$ ) are inhaled but usually remain in the throat or nasal passage with some deposition in the trachea and upper lungs; these are removed via the lining of the respiratory tract. Fine (below  $1 \mu\text{m}$ ) and ultrafine (below  $0.1 \mu\text{m}$ ) particulates enter deep into the respiratory system for which there is no effective removal system [34].

In 2008 the EU established specific directives to regulate the emissions of  $\text{PM}_{10}$  (diameter less than  $10 \mu\text{m}$ ) and  $\text{PM}_{2.5}$ . Establishing a size distribution

of key sources of particulate matter at airports will enable operators to determine whether action needs to be taken to meet the new standards. It will also provide an insight into the associated health risks of living near to or working at an airport.

The following report is in two parts. Part I refers to hygroscopic growth and includes a review of the current state of knowledge and an outline proposal for experimental work. Part II details the study of aviation tyre emissions following fieldwork at Cranfield airport. The results are discussed and a summary of the findings is presented.

## Part I

### 3 Objectives

The aim of this study is to expand upon previous research and propose an experiment to obtain hygroscopic growth curves for ammonium sulphate and ammonium nitrate particles with dry diameters on the micron scale. The predicted increase in emissions of the reactants which produce nitrate aerosol combined with the decrease in ammonium sulphate aerosol means that nitrate aerosol studies are of ever increasing importance. Obtaining hygroscopic growth curves for a range of dry aerosol diameters is relevant to further research into the optical properties of the aerosol solution droplets which are present in atmospheric regions of differing relative humidities.

### 4 Review of current knowledge

Bauer et al (2007) [41] quantify the direct radiative forcing attributable to nitrates at  $-0.11 \text{ Wm}^{-2}$ , with Liao and Seinfeld (2005) [42] determining a value of  $-0.16 \text{ Wm}^{-2}$  and Adams et al (2001) [43] in close agreement measuring  $-0.19 \text{ Wm}^{-2}$ , with a radiative forcing estimate of  $-0.45 \text{ Wm}^{-2}$  for sulphate aerosols [41].

In the gas phase, oxidation of  $\text{NO}_X$  by OH forms nitric acid which is then neutralised in the presence of ammonia to ammonium nitrate. If there is insufficient sunlight then  $\text{NO}_2$  reacts with  $\text{NO}_3$  to form  $\text{N}_2\text{O}_5$  which in the presence of hydrated aerosols is converted to nitric acid [13]. The ammonium sulphate aerosol exists in either liquid form or partly crystallised droplets. The droplets are formed via the oxidation of  $\text{SO}_2$  by OH from ammonia which then condenses onto the pre-existing particles leading to aerosol growth [14]. In the presence of excess  $\text{SO}_2$  and  $\text{NH}_3$ , ammonia will preferentially react to form ammonium sulphate [15]. Current data on atmospheric

composition over Europe details that 10-20% of total dry mass is accounted for by nitrates, with sulphate accounting for 10-30% [16]. The larger partitioning of nitrate aerosol in Europe is due to the reduction of SO<sub>2</sub> emission from 18 TgS yr<sup>-1</sup> in 1980 to 4 TgS yr<sup>-1</sup> in 2002 [17].

The leading source of atmospheric SO<sub>2</sub> is fossil fuel burning (~70% of total emissions), a small proportion is produced from biomass burning (~3%) whilst the most significant natural source is oceanic phytoplankton (~18%) with a sizeable contribution from volcanic activity (~8%) [2]. The main sources of nitrous oxides are fossil fuel burning, lightning and biomass combustion. Emissions of ammonia are highly biased towards anthropogenic sources which are themselves dominated by processes associated with food production. Faeces from domestic animals accounts for 40% of the total global emissions in 1997 (54 TgN yr<sup>-1</sup>) with synthetic fertilisers contributing 17%, in comparison only 0.2% is accorded to wild animal excreta [18].

#### 4.1 Models of hygroscopic growth

Our understanding of the energetics of droplet formation and subsequent hygroscopic growth is based on the work of Köhler [7] which is discussed thoroughly by Pruppacher and Klett [39]. The unique vapour pressure for a liquid at a given temperature is the minimum partial pressure of the vapour of that liquid which must be maintained at the gas-liquid interface to prevent evaporation. The saturation ratio is the ratio of the partial pressure of the vapour to the saturation vapour pressure; when the saturation ratio exceeds one the mixture is described as supersaturated and nucleation occurs [8].

Köhler theory states that the relation between the size and chemical composition of an aqueous droplet and the relative humidity under equilibrium conditions can be described by [23] :

$$S_W = a_W \exp\left(\frac{4\sigma M_W}{\rho R T D_m}\right) \quad (1)$$

The relative humidity,  $RH$  is equal to the water vapour saturation ratio,  $S_W$ , expressed in percent.  $M_W$  is the molar mass of H<sub>2</sub>O;  $T$  is the absolute temperature;  $\rho$  is the density and  $\sigma$  is the surface tension of the aqueous solution.  $R$  is the ideal gas constant.  $a_W$  is the water activity of the solution droplet which is defined as the ratio of equilibrium water vapour pressures over flat surfaces of the aqueous solution and of pure water.

The two competing mechanisms acting to increase and decrease the vapour pressure are known as the

Kelvin effect and the Raoult or solute effect respectively. The Kelvin effect describes the increase in vapour pressure of a pure solvent on a curved surface compared to a flat surface and scales with the inverse of the droplet's geometric diameter,  $D_m$ . The exponential term in the expression above represents the Kelvin effect. The Raoult effect describes the decrease in vapour pressure of a solution which contains a non-volatile solute compared to pure solvent [40]. Theoretical growth is most commonly illustrated by the Köhler curve;  $RH$  plotted against the measured particle diameter. Figure 1 illustrates hygroscopic

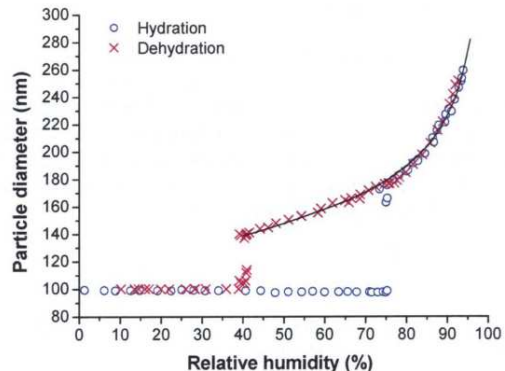


Figure 1: The change in diameter of NaCl particles with dry diameter 99 nm upon hydration and dehydration compared to Köhler theory calculations (solid black line) for particles with dry diameter 95 nm. Results from Mikhailov et al [23].

growth for NaCl and also demonstrates the hysteresis effect which particles exhibit depending on their  $RH$  history. The growth of dry solid particles does not follow the Köhler curve immediately upon hydration but maintains its dry diameter until the deliquescence relative humidity (DRH) is reached. Water soluble aerosols undergo a phase transformation at the DRH, changing from solid to aqueous (droplet) phase and undergoing spontaneous growth. This is illustrated in the figure by the apparent step change in particle diameter from ~100 nm to 160 nm at ~75%  $RH$ . As the  $RH$  is increased beyond the DRH the droplet diameter increases in agreement with the Köhler theory up to 100%  $RH$ . Upon dehydration the droplet's diameter decreases along the Köhler curve beyond the DRH existing as a supersaturated droplet in a metastable equilibrium state [22]. The diameter undergoes another step change during dehydration at the efflorescence relative humidity (ERH) at which the solution droplet crystallises. Figure 1 demon-

strates the phase change at an ERH of  $\sim 40\%$  at which the diameter steps from 140 nm to 120 nm.

## 4.2 Previous study

The IPCC consider the indirect effect of aerosols to be a key uncertainty in the radiative forcing of climate [9]. The direct link between hygroscopic growth of ammonium sulphate and ammonium nitrate with the microphysical properties of clouds indicates the importance of continued study of the water uptake of aerosols. There have been a number of previous studies on the hygroscopic nature of ammonium sulphate [19] [20] [21] [22] which obtained results consistent with the Köhler theory and associated hysteresis effects; the deliquescence transition was observed at  $\sim 80\%$  RH and efflorescence at  $\sim 33\%$  RH. Ammonium nitrate has been the subject of fewer limited studies due to its volatility which tends to result in significant evaporation during the process of dehydration and rehydration [13]. There is some disagreement between the results of recent studies of ammonium nitrate, with discrepancies between different experiments as well as between theoretical and empirical data. Mikhailov et al [23] observed no distinct efflorescence or deliquescence transitions for aerosols with a dry diameter of 99 nm in agreement with Richardson and Hightower [24] and Lightstone et al, who saw no evidence of efflorescence on dehydration of ammonium nitrate to 0% RH. However, Lightstone et al noted a deliquescence point at  $\sim 62\%$  which is in good agreement with the theoretical calculation of 62% RH. Chan et al [44] did observe efflorescence of ammonium nitrate at  $\sim 30\%$  RH which agreed with the data from Tang [45] of ERH between 25 and 32% RH.

Study into the hysteresis effect by Bauer et al [41] concluded that depending on whether the water uptake of the aerosol was controlled via the upper or lower side of the hysteresis loop; the combined radiative forcing of the nitrate/ammonia/sulphate aerosol varied by  $\sim 25\%$ .

## 5 Experimental Proposals

Previous studies typically use a Hygroscopic Tandem DMA (Differential Mobility Analyser) to measure hygroscopic growth. The basic experimental setup follows; a quasi-monodisperse range of dry particulates is selected using a DMA, the dry particulates enter humidifiers at a controlled RH where they undergo hygroscopic growth, a second DMA with an optical particle counter measures the diameter of the droplet

following humidification [46]. The experimental proposal for this study does not use a DMA because these typically only work well for measurements of particles between 20 and 500 nm [47] whereas we aim to measure growth of particulates with a dry diameter on the micron scale. Figure 2 shows a block diagram

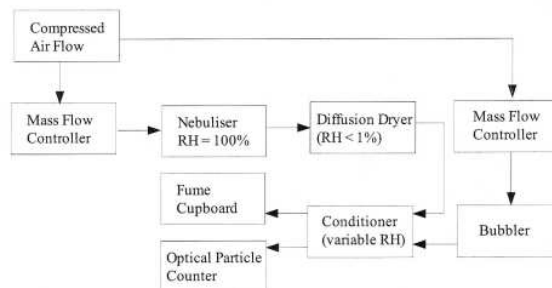


Figure 2: Proposed experimental setup for measuring hygroscopic growth. The aerosols are produced via an ultrasonic nebuliser and dried using a diffusion dryer before undergoing hygroscopic growth in a conditioner. The RH is controlled by a mass flow controller and water bath bubbler. An optical particle counter measures the resulting particle diameter.

of the proposed experimental set-up. The aqueous solutions of ammonium nitrate and ammonium sulphate will be prepared by dissolving the substance in deionised water. The aerosols will be generated by atomisation of the aqueous solution using an ultrasonic nebuliser which uses high frequency vibrations to produce droplets of the same concentration as the aqueous solution. The nitrogen carrier gas flow rate into the nebuliser will be controlled using a mass flow controller. The solution droplets produced by the nebuliser will be quasi-monodisperse and are subsequently dehydrated ( $RH$  less than 1%) by a diffusion dryer which consists of an acrylic tube containing silica gel. The dried particles will have a diameter which can be calculated based on the volume of the droplets produced by the nebuliser and the concentration of the initial aqueous solution of the substance.

To determine the hygroscopic growth the dried particles are hydrated to a known RH within a conditioner. The RH is varied between  $\sim 0\%$  and 100% by varying the flow rate through the water bath bubbler. The diameter of the particles is then measured using an optical particle counter, see part II for details, and would be plotted against RH as in figure 1 for analysis.

## 6 Summary

We have reviewed the current knowledge of hygroscopic growth of ammonium nitrate and ammonium sulphate and their contribution to the climate system. Following our research we have successfully proposed an experiment using a nebuliser and diffusion dryer to obtain hygroscopic growth curves. Enhanced knowledge of the optical properties of aerosols, which relate directly to their hygroscopic nature, will allow improved modelling of the contribution of aerosols to the Earth-atmosphere radiation balance.

## Part II

### 7 Objectives

This study aims to build on the research already completed on automobile tyres to obtain a size distribution of tyre smoke from an aircraft whilst undergoing routine airport manoeuvres (taxi and landing) using an optical particle counter (OPC), condensation particle counter (CPC) and SPARCLE (advanced optical particle counter). The serious implication of the health effects associated with particulate emissions and their specific dependence on the size of the aerosol means that obtaining a size distribution of aircraft tyre particulate emissions is extremely important.

The investigation will also provide an opportunity to field test the optical and electronic system in SPARCLE for an extended period of time. Any results obtained from the instrument will be supplementary to the main experiments.

### 8 Review of current knowledge

Tyre wear is one of the most significant non-engine aviation emissions which contributes to atmospheric aerosol concentrations. Tyre emissions are due to frictional forces between the tyre and ground which occur when the aircraft is in motion, especially during taxi and landing manoeuvres. Larger solid material is deposited on the runway surface whilst the smaller matter becomes suspended in the air [32].

The planned expansion of London Heathrow Airport (LHR) has prompted new investigation into atmospheric aviation emissions in order to gauge the environmental impact of the proposed increase in capacity. Prior to 2000 there was no quantitative research on the contribution of tyre wear and brake emissions to the total emissions estimate. The LHR

emissions inventory in 2002 assumed that all of the tyre material deposited was of the PM<sub>10</sub> size range (diameter less than 10  $\mu\text{m}$ ) [31]. A British Airways study (2006) [35] determined a tyre mass loss range of 0.078 kg to 0.812 kg per landing for aircraft of landing mass 68 000 kg to 400 000 kg. This result was obtained by calculating the mass difference between new and worn tyres and dividing through by the number of landings. Approximately 1300 landings occur at Heathrow per day [33] which would deposit between 101 kg and 1 055 kg of tyre particulate matter based on these findings.

A number of studies have been carried out relating to automobile tyre wear, with Cadle (1978) determining that the dispersed tyre particle size range was between 0.01 and 30  $\mu\text{m}$  [36] whilst Miguel et al (1999) [37] determined that 50 - 70% of airborne road side dust is PM<sub>10</sub>.

Despite the recent increase in the number of studies the Airport Cooperative Research Program (ACRP) [34] considers that

the present understanding of particle properties is insufficient to evaluate the health and environmental effects from exposure to different types and sizes of particulate matter.

This is in agreement with Underwood et al (2002) [31] who stated that the data produced from automobile studies should be treated with caution in relation to their relevance to aircraft emissions.

### 9 Experimental Method

Data was collected from 8 sorties; consisting of taxi, take-off and landing of a BAE-146 (see appendix, figure 14) aeroplane at FAAM (Facility for Airborne Atmospheric Measurements) located at Cranfield Airport, Bedfordshire. Meteorological conditions initially delayed the investigation from the week commencing 2 February 2009 to the week commencing 16 February 2009. The pre-flight briefing was given on 16 February by FAAM with colleagues from the University of Manchester and University of Cambridge also in attendance. All data was collected on 17 February between 09:00 and 15:00 during two flights consisting of 4 sorties commencing at  $\sim$ 10:00 and 13:00.

The experimental set up consisted of SPARCLE which provided data on the size, number and optical properties of the aerosol particulates, an OPC gathered data on particle size and number and a CPC provided data on particle number (see figure 3). The

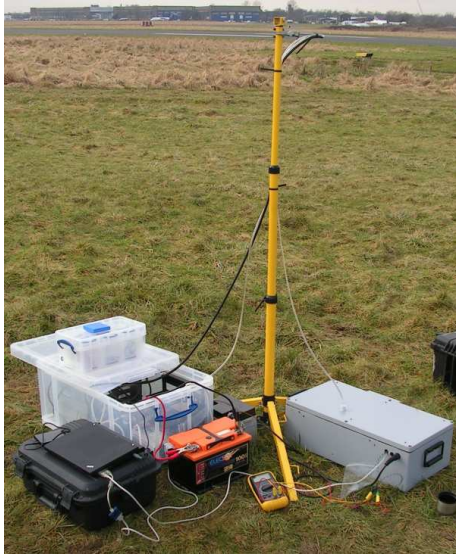


Figure 3: Instrument setup; the OPC and CPC were situated within the plastic box on the left, SPARCLE is the grey box to the right. The inlets are attached to the yellow tripod.

instruments collected aerosol particles through separate inlets (see figure 3). In the OPC, the stream of particles passes through a laser illuminated optical system; individual particulates scatter the light beam and these scattered pulses are detected by a solid state detector. Electronics within the system amplify and record the number of pulses detected, corresponding to the number of particles per cc based on the inlet flow rate [25]. The efficiency of the OPC sampling system is determined by the inlet parameters; flow rate  $11 \text{ min}^{-1}$ , diameter 3.2 mm and length 1515 mm. The OPC detects particles with a lower limit diameter of  $0.3 \mu\text{m}$ .

A CPC provides data on the total number of particles below  $3 \mu\text{m}$  diameter by growing the aerosol particulates to a size which is optically detectable. The aerosol particles are grown via condensation of a supersaturated vapour onto their surface [26]. The optical detection system and electronics are the same as for the OPC. The inlet had a flow rate of  $300 \text{ ml min}^{-1}$ , diameter 6 mm, length 2217 mm ( $\pm 5 \text{ mm}$ ).

SPARCLE determines particle count by detecting the aerosol scattered laser pulses. The optical properties and size of the aerosol are extracted by measuring the scattering angle of the signal using a linear detector array. SPARCLE inlet parameters; flow rate  $0.0251 \text{ min}^{-1}$ , diameter 3.2 mm and length 1555 mm.

The wind direction and position of the instruments

are shown in figure 4. The instrument location was selected to be down wind of the emissions and a safe distance from the runway. The measured average wind speed for the duration of the experiments was  $4 \text{ ms}^{-1}$ ; the direction varied slightly but remained approximately north westerly (approximately perpendicular to the runway).



Figure 4: Aerial photograph showing approximate landing locations by sortie no., wind direction and instrument position.

## 10 Results and Discussion

### 10.1 CPC

The particle concentration data for sortie 7 obtained by the CPC is displayed in figure 5 (see appendix, figure 15 for all sorties). The event markers denote the onset of the smell of kerosene or tyre smoke at the inlet location as detected by the instrument operators. The data showed that an aerosol plume of particulates with diameter less than  $3 \mu\text{m}$  was produced by the aircraft during taxi, take-off and landing. The time delay between the event markers and the particle count peaks is due to the travel time of the aerosol along the pipe from the inlet to the instrument. The expected travel time of  $\sim 13 \text{ s}$  was calculated by my colleague based on the flow parameters which is in good agreement with the average measured delay of  $\sim 15 \text{ s}$ .

The highest particle concentrations were detected during the aircraft taxi for all sorties except for sortie 1 where the peak particle concentration occurred during take-off. The aerosol plume peak count was between  $6 \times 10^5 \text{ cm}^{-3}$  and  $8 \times 10^5 \text{ cm}^{-3}$  for all taxis except for those during sorties 1 and 3 where the particle count was only  $\sim 5 \times 10^5 \text{ cm}^{-3}$ . The aircraft take-off

plumes were detected between between  $3 \times 10^5 \text{ cm}^{-3}$  and  $5 \times 10^5 \text{ cm}^{-3}$  in sorties 2 to 8 whereas for sortie 1 the peak was almost  $6 \times 10^5 \text{ cm}^{-3}$ . These variations are most likely due to changing wind speed and direction and the position of landing relative to the inlets, see appendix for further discussion.

For taxi and take-off the particle plumes are attributed to emissions from the engine exhaust; it was also noted that instrument operators observed a distinct smell of kerosene. Whilst taxiing the aircraft uses only 13% of the fuel which is required for take-off [27]. The higher particle count observed during taxi despite the lower fuel consumption implies that the plume is dispersed more greatly by the dynamics of the plane's motion on take-off than whilst taxiing. The aircraft's speed on taxi is  $\sim 30 \text{ km h}^{-1}$  [28] whilst the aircraft accelerates to a speed of  $\sim 250 \text{ km h}^{-1}$  whilst on the runway during take-off [29] which would lead to a greater horizontal dispersion of the aerosol plume. The aircraft wings create lift on take-off which would also cause vertical dispersion of the plume.

Landing plumes were observed with a peak particle count between  $1 \times 10^5 \text{ cm}^{-3}$  and  $2 \times 10^5 \text{ cm}^{-3}$  which was much lower than for taxi and take-off. As can be observed in figures 5 and 15 (in appendix) the peaks representing aerosol plumes on landing were much broader than those for taxi and take-off and they also contained distinct sub-peaks. For sorties 2, 4, 6, 7 and 8; 2 sub-peaks indicating increased particle concentration were clearly observed at the beginning and end of the aerosol landing plume. This effect was probably due to the two wing vortices which are columns of rapidly circulating air created when a wing generates lift [30].

It is likely that the sub-peaks were not present in the plumes during take-off because the instruments were located towards the far end of the runway. Therefore, the aircraft passed the inlets at a much lower speed compared to during landing thus much less lift was generated by the wings.

The background particle concentration is not evident in figure 5 as it was only  $\sim 5 \times 10^3 \text{ cm}^{-3}$  throughout the 6 hour period which was two orders of magnitude smaller than the peak concentrations. Tyre smoke emission was visible to the eye during landing (see figure 6) whereas the engine emissions were not observed photographically. This implied that tyre smoke particulates are much coarser than engine emissions and therefore would not have been detectable by the CPC. The LIDAR instrument deployed by colleagues from University of Manchester detected tyre smoke during landing for 6 out of 8 sorties [27]. The detection times of tyre smoke from the LIDAR were checked against the CPC data however,

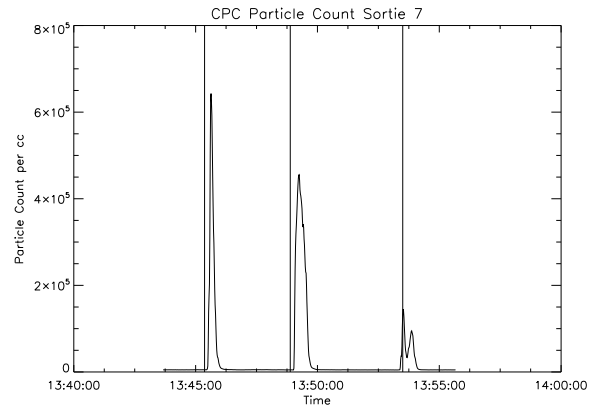


Figure 5: CPC data for sortie 7. Vertical lines are event markers of when kerosene or tyre smoke smell was detected at inlets. Peaks left to right correspond to taxi, take-off and landing.

there was no significant CPC signal above background count at these instances. Therefore, we suggest that the aerosol plume detected by the CPC during landing was due to engine emissions.



Figure 6: Photograph of sortie 6 landing. Minimal tyre smoke is visible behind the wheels.

## 10.2 OPC

The OPC data (see figure 7) was summed over all size bins therefore the signal is proportional to the total particle concentration. A top hat function was passed through the data to smooth and reduce noise. No distinct peaks in the OPC data are observed and there was no correlation between the event markers and the signal. Therefore no plumes of particulates with diameters exceeding  $0.3 \mu\text{m}$  were detected.

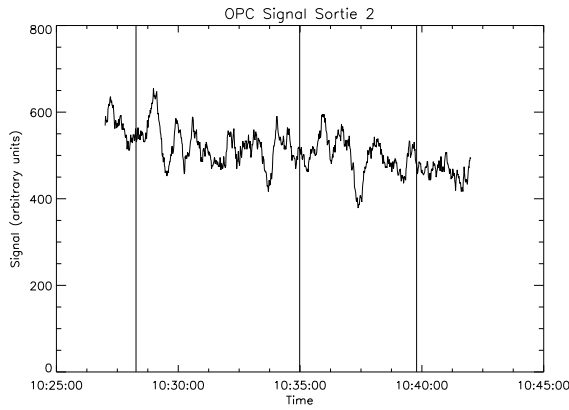


Figure 7: OPC data for sortie 2. Vertical lines are event markers for detection of kerosene or tyre smoke smell at inlets. Signal (arbitrary units) is proportional to total particle count per cc of aerosols with diameter greater than  $0.3 \mu\text{m}$ .

The variation in OPC signal shown in figure 7 was due to the variation in ambient aerosol concentration. Figure 16 (see appendix) shows that the overall OPC signal decreased from 550 at 10:30 to 150 (arbitrary units) for 12:30 onwards. This indicates a decrease in ambient aerosol concentration which was in agreement with increased visibility.

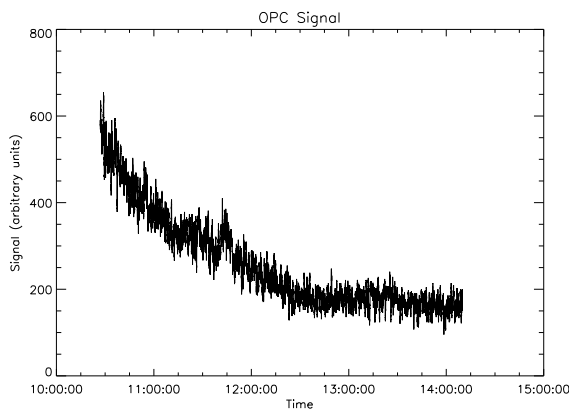


Figure 8: Continuous OPC data for the duration of the sorties. Signal (arbitrary units) is proportional to total particle count per cc of aerosols with diameter greater than  $0.3 \mu\text{m}$ .

### 10.3 SPARCLE

SPARCLE recorded the time elapsed between each new particle detected by the optical system. To pro-

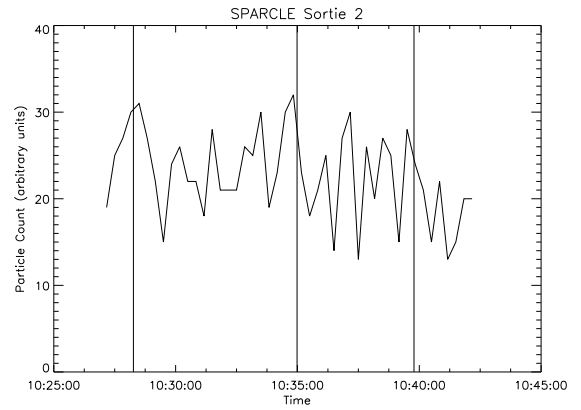


Figure 9: SPARCLE data for sortie 2. Particle count axis has undefined units; the signal is proportional to particle count per cc of aerosols with diameter greater than  $0.3 \mu\text{m}$ . Vertical lines are event markers.

duce a signal which is proportional to particle count per cc with respect to time, the time between events (particles) was converted into the actual time of the event in Julian time. The number of events within 20s was then calculated with a time stamp being defined as the midpoint of the time period in Julian time. The data in figure 9 showed no peaks or aerosol plumes associated with the noted times of taxi, take-off and landing. The variation observed in particle count is attributed to the ambient aerosol fluctuation throughout the day. SPARCLE uses a linear detector

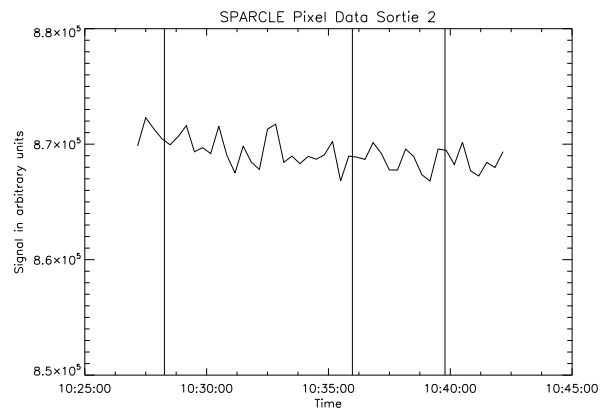


Figure 10: SPARCLE pixel data for sortie 2. Vertical lines are event markers of when kerosene or tyre smoke smell was detected at inlets. The signal is proportional to particle diameter.

array to provide data on the size of the aerosols sam-

pled by determining the angle through which light is scattered by the particle. For a larger diameter particle the array will detect a signal in a greater number of its pixels therefore the total signal intensity, which was the sum across all pixels at a given time, can be interpreted as proportional to particle size. The pixel data was then smoothed to reduce background noise. We interpret from figure 10 that there is no significant change in the size of particles sampled by SPARCLE throughout the sorties. This is consistent with the data from the OPC.

For the first 4 sorties which took place between 09:55 and 11:25 the average pixel signal was between  $8.6 \times 10^5$  and  $8.8 \times 10^5$  (arbitrary units). The second 4 sorties occurred between 13:00 and 14:20 and the average signal for these was between  $8.5 \times 10^5$  and  $8.6 \times 10^5$  (arbitrary units). This indicates that average particle size of the sampled aerosols decreased in the afternoon compared to the morning. This was expected due to the sky becoming noticeably clearer throughout the day which would suggest a decrease in the concentration and also size of suspended hygroscopically grown droplets in the air. Figure 11

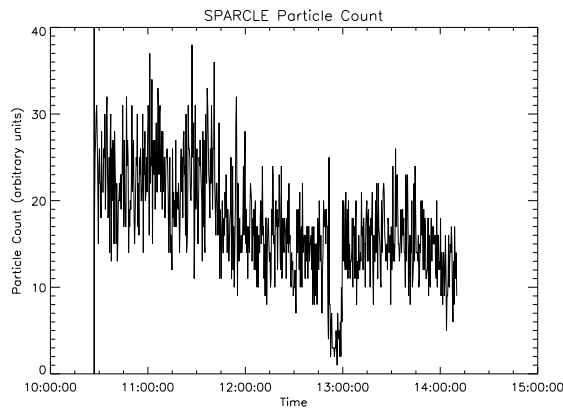


Figure 11: Continuous SPARCLE data for the duration of the sorties. Particle count axis is in undefined units and is proportional to particle count per cc of aerosols with diameter greater than  $0.3 \mu\text{m}$ .

displays the particle count data from SPARCLE for the entire 6 hour period for which the instruments were in operation. The data clearly showed the predicted decrease in ambient aerosol concentration from 25 at 10:30 to 13 (arbitrary units) at 14:30. This also agreed with the data from the OPC in figure 8 and provided good evidence that SPARCLE was operating correctly. The significant drop in particle count observed at 13:00 was when the zero filter was placed on the SPARCLE inlet.

The experiment was considered a success as a field test for SPARCLE. The instrument operated correctly for the entire 6 hour period of investigation producing both particle size and count data. The initial results are in agreement with the OPC and work will now continue into developing the method of data analysis following the success of the instrument hardware.

## 10.4 Laboratory Work

### 10.4.1 Size Distribution

Field work at Cranfield did not provide sufficient data to determine a size distribution of tyre emissions. Therefore, a laboratory investigation on a sample of tyre and brake brushings from the underside of the aircraft (collected on 16/10/08) was conducted.

An aerosol disperser and sizer (see figure 13) was used to obtain a size distribution. The aerosol disperser used an air pump to disperse the sample of particulates through a dispersing pin. The shear force exerted on the particulate sample was varied by altering the pressure drop across the dispersing pin. A higher shear force would increase the deagglomeration of the sample thus allowing the fine aerosol constituents to be detected.

The aerosol disperser has two modes for varying the air flow speed at which the particles are transported from the sample container to the dispersing pin; normal deagglomeration and high deagglomeration. The high deagglomeration mode results in the particulates travelling at a greater velocity and therefore results in higher impaction energy, which causes a greater separation of the aerosol. The dispersed aerosol is then transported to the aerosizer via tubing. The aerosizer determines the size of a individual particle by measuring the time taken for it to traverse two laser beams after passing through a supersonic flow region. Figure 12 shows that the tyre and brake sample contained aerosols which were dispersed into particulates between  $0.7 \mu\text{m}$  and  $135 \mu\text{m}$ . Peaks are evident in the overall size distribution at  $\sim 1.2 \mu\text{m}$ ,  $7.0 \mu\text{m}$  and  $35 \mu\text{m}$  diameters. We interpret these peaks as belonging to the size distributions of individual constituents of tyre and brake emissions. It is also evident from the data that most of the dispersed mass is within the  $35 \mu\text{m}$  particulates.

In relation to the new EU directives we have determined the percentage mass contribution of  $\text{PM}_{10}$  and  $\text{PM}_{2.5}$  in the sample. We find that  $\sim 0.1\%$  by mass is classed as  $\text{PM}_{10}$  with only  $\sim 10^{-4}\%$  in the  $\text{PM}_{2.5}$  category. This is encouraging considering that only particulates of diameter less than  $1 \mu\text{m}$  would be

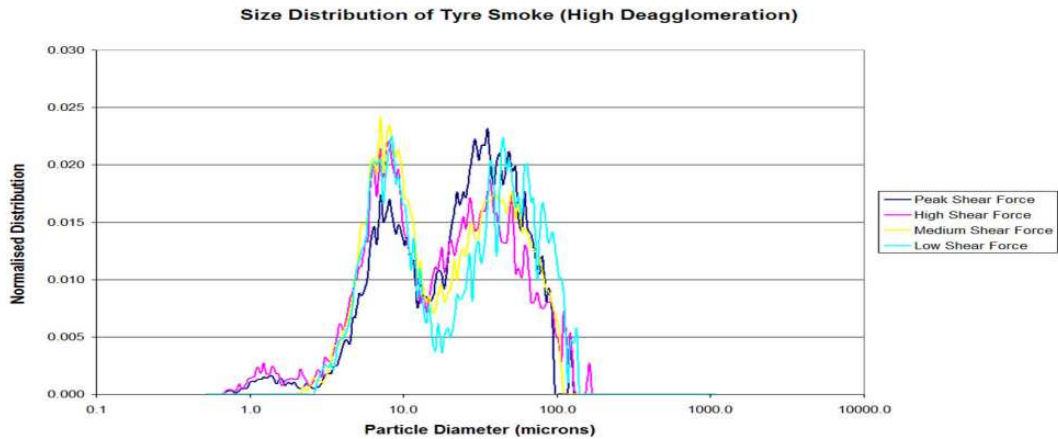


Figure 12: Size distribution of tyre and brake brushings sample (16/10/08) from undercarriage of BAE-146 displaying 3 distinct peaks at approximately  $1.2\ \mu\text{m}$ ,  $7.0\ \mu\text{m}$  and  $35\ \mu\text{m}$  diameters.

deposited deep in the lungs which could lead to long term health effects. The larger particulates would be deposited either in the nose, throat or trachea where efficient removal mechanisms prevent subsequent movement to the deep lung region.

The method used for obtaining this sample must be considered in relation to whether the results are representative of the real time deposition of tyre particulate matter. The sample was removed from the undercarriage of the aircraft which implies some preferential selection as the matter must have been able to adhere to the metalwork. It was also noted during the sample preparation that it contained matter other than tyre, including runway grit. However, considering that our instruments did not detect any tyre  $\text{PM}_{2.5}$  at Cranfield; it is promising that we determined a size distribution which peaked for coarse PM.

#### 10.4.2 Aerosol Transportation and Sampling Efficiency

The tyre material dispersed on landing would have undergone gravitational settlement thus limiting the size of particle which was transported to the instrument inlet. The larger particles have a higher settling velocity which would have resulted in them settling below the inlet height at the instrument location. The settling velocity is calculated via iteration of the equation for gravitational settling of particulates which is discussed in Willeke and Baron [48].

The GPS position of the instruments located the inlets at  $\sim 85\ \text{m}$  from the approximate positions of the aircraft's rear wheels on touchdown. The average wind speed was  $4\ \text{ms}^{-1}$  in a direction perpendicular to

the runway. It was assumed that the aerosol was dispersed to a height of 2 m by the tyres during landing and that the inlets were at a height of 1.5 m. Calculation of the particle range assumed that horizontal transportation was dependent on the wind speed and the settlement time for the 0.5 m height difference between dispersal and the inlets.

Application of this method determined that the critical diameter was  $28\ \mu\text{m}$ ; particulates below this size had a transportation range exceeding the landing to inlet distance. Therefore, the particles contained within the peak at  $35\ \mu\text{m}$  (figure 12) would have settled below the height of the inlets before reaching their location. Thus, they would not have been sampled which is in agreement with the absence of peaks in the OPC or SPARCLE data.

Efficiency curves for the instrument inlets were produced by my colleague and are presented in the appendix (see figure 20). Applying the conventional practice of classifying inlets as inefficient for aerosol sampling when the efficiency is below 0.5; we interpret that the CPC and OPC are inefficient for particles of diameter exceeding  $\sim 10\ \mu\text{m}$  and SPARCLE is only efficient up to  $\sim 7\ \mu\text{m}$ . Combining this with our size distribution data we find that the OPC and CPC inlets would only sample  $\sim 0.1\%$  by mass of emissions similar to our test sample. SPARCLE would only be classed as efficient for 0.03% of the tyre particulate matter by mass.

## 11 Summary and Further Work

In this study an optical particle counter, condensation particle counter and the newly developed SPARCLE instrument were used to measure aircraft aerosol emissions. The aerosol plumes were characterised during eight sorties of a BAE-146 with 4 jet engines.

The CPC provided data on aerosols with a diameter of less than  $3\ \mu\text{m}$  and showed clear evidence of aerosol plumes during taxi, take-off and landing. The particle counts measured by the CPC during taxi were primarily between  $6 \times 10^5\ \text{cm}^{-3}$  and  $8 \times 10^5\ \text{cm}^{-3}$  whilst those on take-off were between  $3 \times 10^5\ \text{cm}^{-3}$  and  $5 \times 10^5\ \text{cm}^{-3}$ . These plumes have been attributed to emissions from the aircraft engines due to their fineness and the kerosene smell which was identified at the inlet site by the instrument operators.

The LIDAR from colleagues at University of Manchester detected tyre smoke on 6 landings out of 8 sorties however, the times at which this occurred were not in agreement with the aerosol plumes detected by the CPC. Therefore, it has been concluded that tyre smoke was not detected by the CPC and that the landing plumes were also attributed to engine emissions. However, it was noted that the smell produced on landing was distinct from the kerosene smell observed during taxi and take-off therefore, an additional fine aerosol must have been produced although not detected by the instruments.

Neither SPARCLE nor the OPC showed any evidence of aerosol plumes associated with the aircraft's movements, however the ambient aerosol concentration was observed to decrease. SPARCLE operated correctly for 6 hours and the field test was considered a success.

Study of a sample of tyre and brake emission brushings using an aerosol disperser and aerosizer obtained a size distribution with 3 distinct peaks (see figure 12) at diameters of  $\sim 1.2\ \mu\text{m}$ ,  $7.0\ \mu\text{m}$  and  $35\ \mu\text{m}$ . With regard to the recent EU standards on particulate emissions; the percentage by mass of  $\text{PM}_{10}$  was found to be 0.1% and  $10^{-4}\%$  within  $\text{PM}_{2.5}$ .

Investigation into aerosol transportation suggested that gravitational settlement would have prevented aerosols exceeding  $\sim 28\ \mu\text{m}$  in diameter from reaching the instrument location. In addition, study into the inlets demonstrated that the CPC and OPC were only efficient up to  $10\ \mu\text{m}$  and SPARCLE up to  $7\ \mu\text{m}$ . Considering that  $\text{PM}_{10}$  is likely to have contributed only 0.1% by mass to the emissions it is probable that the amount of tyre aerosol produced on landing was not large enough to be detected above the ambient aerosol concentration of  $\sim 5 \times 10^{-3}\ \text{cm}^{-3}$ . The lack

of tyre smoke may be attributed to the significant age of the tyres.

Proposals for further work:

- Optimise the instrument inlets to sample most efficiently at the peak diameters ( $1.2\ \mu\text{m}$ ,  $7.0\ \mu\text{m}$ ,  $35\ \mu\text{m}$ ) obtained from the laboratory investigation.
- Calibrate SPARCLE signal against known particulate size distributions and develop its refractive index measurement to enable signal to be extracted from background noise.
- Investigate the relationship between age of tyres and the amount and size distribution of tyre PM deposited on landing.
- It is known that tyres contain black carbon, organic carbon, polycyclic aromatic hydrocarbons and some metals. The chemical composition of the individual peaks in the size distribution of dispersed tyre PM needs to be determined with particular focus on the content of  $\text{PM}_{10}$ .

## 12 Conclusion

The first study proposed an outline experimental setup to determine the hygroscopic growth of ammonium nitrate and ammonium sulphate aerosols. Further study is required to implement the method and compare the results with the theoretical values from the Köhler theory.

In part II, the main purpose of the investigation was to obtain a size distribution of aircraft tyre emissions during landing. The study was unsuccessful in producing a size distribution from real time data gathered at Cranfield airport. The secondary objective to field test SPARCLE was a success although the data did not supplement our findings.

The investigation was carried out with reference to the recent EU directives which limit the emission of  $\text{PM}_{2.5}$  and  $\text{PM}_{10}$ . The laboratory study of the tyre and brake emissions sample determined that over 99% of the particulate matter by mass was larger than  $\text{PM}_{10}$  and thus would not contribute to any serious health risks posed by particulate matter inhalation. Although thorough research into the composition of the individual aerosols which are dispersed upon landing is required; this study has succeeded in adding to the currently limited knowledge of aircraft tyre emissions.

## References

- [1] Wayne, R. P.: Chemistry of Atmospheres (Oxford University Press, 2000), p7.
- [2] Haywood, J. M. and Boucher, O.: Estimates of the direct and indirect radiative forcing due to tropospheric aerosols: A review, *Rev. Geophys.*, **38**, 514-517, 2000.
- [3] Tang, I. N., Tridico A. C. and Fung K. H.: Thermodynamic and optical properties of sea salt aerosols, *J. Geophys. Res.*, **102**, 23,269-23,275, 1997.
- [4] Satheesh, S. K. and Moorthy, K.: Radiative effects of natural aerosols: A review, *Atmos. Environ.*, **39**, 2089-2110, 2004.
- [5] Manton, M. J.: The physics of clouds in the atmosphere, *Rep. Prog. Phys.*, **46**, 1393-1444, 1983.
- [6] Martinsson, B. G. et al.: Droplet nucleation and growth in orographic clouds in relation to the aerosol population, *Atmos. Research*, **50**, 289-315, 1999.
- [7] Köhler, H.: The nucleus in the growth of hygroscopic droplet, *Trans. Faraday Soc.*, **32**, 1152-1161, 1936.
- [8] Willeke, K., and Baron, P. A.: Aerosol Measurement: Principles, Techniques and Applications (John Wiley and Sons 1992), p40-43.
- [9] IPCC 2007 Chapter 2, Changes in atmospheric constituents and in radiative forcing.
- [10] Costa, M. H. and Foley, J. A.: Combined effects of deforestation and double atmospheric CO<sub>2</sub>-concentrations on the climate of Amazonia, *J. Climate*, **13**, 18-34, 2000.
- [11] Soon, W., Baliunas S., Idso, S. B., Kondratyev, K. Y. and Posmentier E. S.: Modelling climate effects of anthropogenic carbon dioxide emissions: unknowns and uncertainties, *Clim. Res.*, **18**, 259-275, 2001.
- [12] Meehl, G. A., Stocker, T. F., Collins, W. D., Friedlingstein, P., Gaye, A. T., Gregory, J. M., Kitoh, A., Knutti, R., Murphy, J. M., Noda, A., Raper, S. C. B., Watterson, I. G., Weaver, A. J. and Zhao, Z.-C.: Global Climate Projections. In: Climate Change 2007: The Physical Science Basis. Contribution of Working Group to the Fourth Assessment Report of the Intergovernmental Panel on Climate Change, 2007.
- [13] Lightstone, J. M., Onasch, T. B., Imre, D. and Oatis, S.: Deliquescence, efflorescence, and water activity in ammonium nitrate and mixed ammonium nitrate/succinic acid microparticles, *J. Phys. Chem. A*, **104**, 9337-9346, 2000.
- [14] Penner, J. E et al.: Aerosols, their direct and indirect effects. In: Climate Change 2001: The Scientific Basis. Contribution of Working Group I to the Third Assessment Report of the Intergovernmental Panel on Climate Change.
- [15] Myhre, G., Grini, A. and Metzger, S.: Modelling of nitrate and ammonium-containing aerosols in the presence of sea salt, *Atmos. Chem. Phys.*, **6**, 4809-4821, 2006.
- [16] Putaud, J.P., Raes, F., Van Dingenen, R. et al.: A European aerosol phenomenology 2: chemical characteristics of particulate matter at kerbside, urban, rural and background sites in Europe, *Atmos. Environ.*, **38**, 2579-2595, 2004.
- [17] Vestreng, V., Adams, M. and Goowin, J.: Inventory Review 2004: Emission Data reported to CLRTAP and the NEC Directive. EMEP/EEA Joint Review Report, Norwegian Meteorological Institute, Norway
- [18] Bouwman, A. F., Lee, D. S., Asman, W. A. H., Dentener, F. J., Hoek, K. W. V. D., and Olivier, J.: A Global High-Resolution Emission Inventory for Ammonia, *Global Biogeochem. Cycles*, **11**, 561-587, 1997.
- [19] Tang, I. N. and Munkelwitz, H. R.: Water activities, densities, and refractive indices of aqueous sulfates and sodium nitrate droplets of atmospheric importance, *J. Geophys. Res.*, **99**, 18,801-18,808, 1994.
- [20] Colberg, C. A., Luo, B. P., Wernlie, H., Koop, T. and Peter, T.: A novel model to predict the physical state of atmospheric H<sub>2</sub>SO<sub>4</sub>/NH<sub>3</sub>/H<sub>2</sub>O aerosol particles, *Atmos. Chem. Phys.*, **3**, 909-924, 2003.
- [21] Kreidenweis, S. M., Koehler, K., DeMott, P. J., Prenni, A. J., Carico, C. and Ervens, B.: Water activity and activation diameters from hygroscopicity data - Part I: Theory and application to inorganic salts, *Atmos. Chem. Phys.*, **5**, 1357 - 1370, 2005.
- [22] Gysel, M., Weingartner, E. and Baltensperger, U.: Hygroscopicity of aerosol particles at low temperatures, 2. Theoretical and experimental

- hygroscopic properties of laboratory generated aerosols, *Environ. Sci. Technol.*, **36**, 63-68, 2002.
- [23] Mikhailov, E., Vlasenko, S., Niessner, R. and Pöschl, U.: Interaction of aerosol particles composed of protein and salts with water vapour: hygroscopic growth and microstructural rearrangement, *Atmos. Chem. Phys.*, **4**, 323-350, 2004.
- [24] Richardson, C. B. and Hightower, R. L.: Evaporation of ammonium nitrate particles, *Atmos. Environ.*, **21**, 971-975, 1987.
- [25] <http://aerosol.ees.ufl.edu/opc/section03.html>
- [26] Hämeri, K., Koponen, I. K., Aalto, P. P. and Kulmala, M.: The particle detection efficiency of the TSI-3007 condensation particle counter, *Aerosol Science*, **33**, 1463 - 1469, 2002.
- [27] AETIAQ
- [28] <http://www.globaltransva.de/Technik/bae146200/info/BAe-146.pdf>
- [29] <http://www.airnewzealand.co.nz/aboutus/fleet/aircraftstatistics.htm>
- [30] <http://www.aviationearth.com/Theory/wingtipvortices.html>
- [31] Underwood, B. Y., Walker, C. T. and Peirce, M. J.: Heathrow Emission Inventory 2002: Part 1: A report produced for BAA Heathrow, netcen/AEAT/ENV/R/1657/Issue 4, 2004.
- [32] Curran, R. J.: Method for estimating particulate emissions from aircraft brakes and tyres. Technical Report, QINETIQ/05/01827, QinetiQ Ltd., 2006.
- [33] Planes 'fly empty' to keep slots at Heathrow, [www.timesonline.co.uk/tol/travel/news/article4340518](http://www.timesonline.co.uk/tol/travel/news/article4340518)
- [34] Webb, S., Whitefield, P. D., Miake-Lye, R. C., Timko, M. T. and Thrasher, T. G.: ACRP report 6: Research needs associated with particulate emissions at airports, Technical Report, Transportation Research Board, 2008.
- [35] Morris, K. M.: An estimation of the material erosion from measurements of aircraft tyre wear, *EJT/KMM/1131/14.18*, British Airways, 2006.
- [36] Cadle, S. H. and Williams, R. L.: Gas and particle emissions from automobile tyres in laboratory and field studies, *Rubber Chemistry and Technology*, **52**(1), pp146-158, 1978
- [37] Miguel, A. G., Cass, G. R., Glovsky, M. M.: Allergens in paved road dust and airborne particles, *Environmental Science and Technology*, **33**, pp 4159-4168, 1999
- [38] Air Quality Guidelines: Global Update 2005. Particulate matter, ozone, nitrogen dioxide and sulphur dioxide. World Health Organisation, 2005.
- [39] Pruppacher, H. R. and Klett, J. D.: *Microphysics of clouds and precipitation*, 2nd ed., Kluwer Academic Publishers, Dordrecht, 1997.
- [40] Lee, W. -M. G., Huang, W. -M. and Chen, Y. -Y.: Effect of relative humidity on mixed aerosols in the atmosphere, *J. of Env. Sci. and Health, A* **36**, pp 533-544, 2001.
- [41] Bauer, S. E., Koch, D., Unger, N. Metzger, S. M., Shindell, D. T, and Streets, D. G.: Nitrate aerosols today and in 2030: a global simulation including aerosols and tropospheric ozone, *Atmos. Chem. Phys.*, **7**, pp 5043-5059, 2007.
- [42] Liao, H. and Seinfeld, J. H.: Global impacts of gas-phase chemistry-aerosol interactions on direct radiative forcing by anthropogenic aerosols and ozone, *J. Geophys. Res.*, **110**, D18208, doi:10.1029/2005/JD005907, 2005.
- [43] Adams, P. J., Seinfeld, J. H., Koch, D., Mickely, L., and Jacob, D.: General circulation model assessment of direct radiative forcing by the sulphate-nitrate-ammonium water inorganic aerosol system, *J. Geophys. Res.*, **106**, pp1097-1112, doi:10.1029/2000JD900 512, 2001.
- [44] Chan, C. K., Flagan, R. C., Seinfeld, J. H.: Water activities in ammonium nitrate/ammonium sulphate solutions, *Atmos. Environ.*, **26A**, 1661-1673, 1992.
- [45] Tang, I. N.: Chemical and size effects of hygroscopic aerosols on light scattering coefficients, *J. Geophys. Res.*, **101**, 19 245 - 19 250, 1996.
- [46] Svenningsson, B. et al: Hygroscopic growth and critical supersaturations for mixed aerosol particles of inorganic and organic compounds of atmospheric relevance, *Atmos. Chem. Phys.*, **6**, 1937-1952, 2006.
- [47] Chen, D. -R., Li, W., Cheng, M. -D.: Development of a multiple-stage differential mobility analyzer, *Aerosol Science and Technology*, **41**, 2, 217-230, 2007.

[48] Willeke, K., and Baron, P. A.: Aerosol Measurement: Principles, Techniques and Applications (John Wiley and Sons 1992), p33.

## 13 Appendix

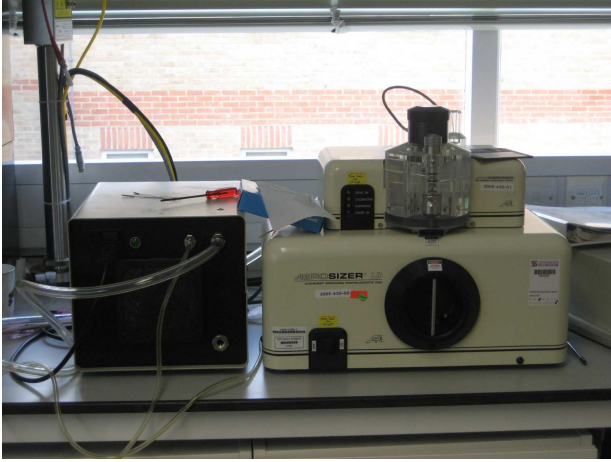


Figure 13: Photograph of apparatus used to obtain tyre sample size distribution. The pump (left) provides the air flow to draw the sample through the aerodisperser (clear cylinder on top of apparatus to the right) which includes a dispersing pin. The aerosizer (bottom right) determines the size of the particulates and the data is fed to a computer.



Figure 14: Photograph of BAE-146 used for field experiments at Cranfield airport, Bedfordshire.

The approximate positions where the back wheels of the plane touched down on landing for each sortie

are shown in figure 4. The variation in landing positions is of the order of  $10^2$  m. It is expected that a greater distance between landing and the instrument inlets would reduce the maximum measured particle count per cc due to dispersion of the particulates both horizontally and vertically. Similarly, the position of each landing relative to wind direction would influence the particle concentration; a lower particle count per cc is expected for landings downwind of the inlets. Table 1 displays the data on peak particle count for each sortie. Further investigation using this data, instantaneous wind speeds and landing positions may provide additional information on aerosol transportation.

Sortie No.	Peak Particle Count per cc
1	184000
4	151000
7	145000
2	133000
8	132000
3	112000
6	111000
5	95000

Table 1: Landing emission peak particle count per cc, in descending order.

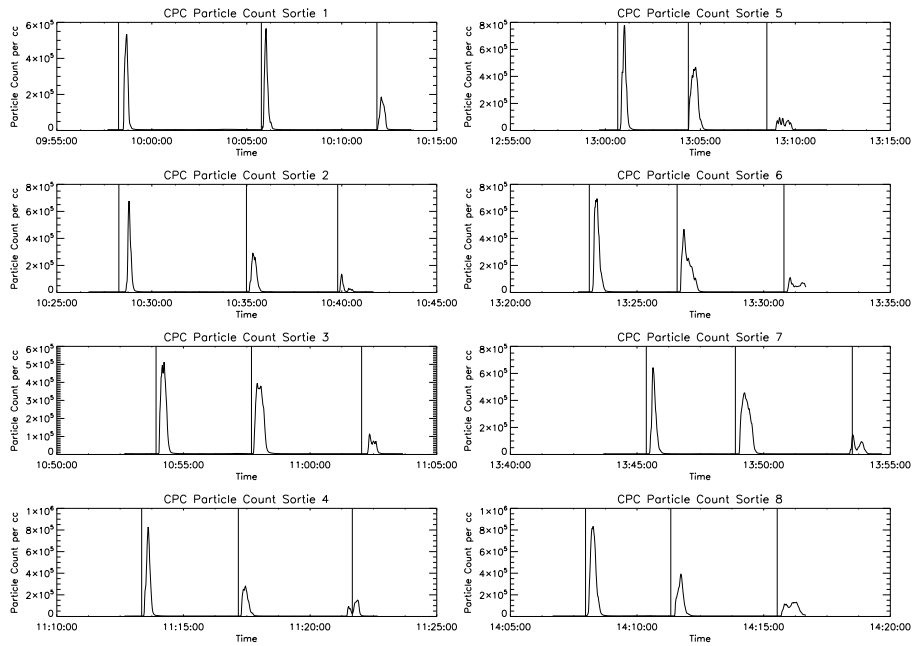


Figure 15: CPC data for all sorties. Vertical lines are event markers of when kerosene or tyre smoke smell was detected at inlets. Peaks left to right correspond to taxi, take-off and landing for each sortie.

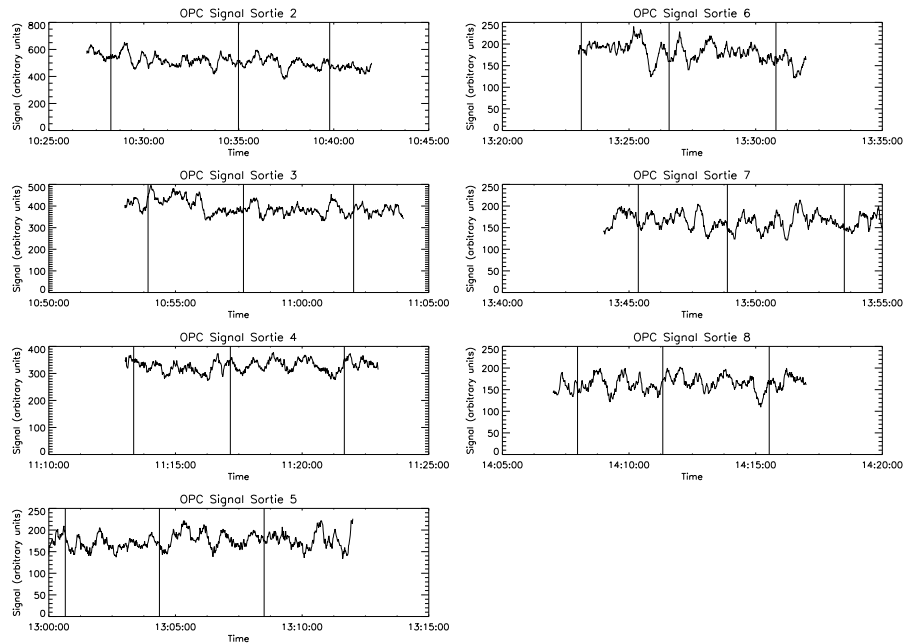


Figure 16: OPC data for all measured sorties (data for sortie 1 unavailable). Vertical lines are event markers of when kerosene or tyre smoke smell was detected at inlets. Signal (undefined units) is proportional to total particle count per cc of aerosols with diameter greater than  $0.3 \mu\text{m}$ .

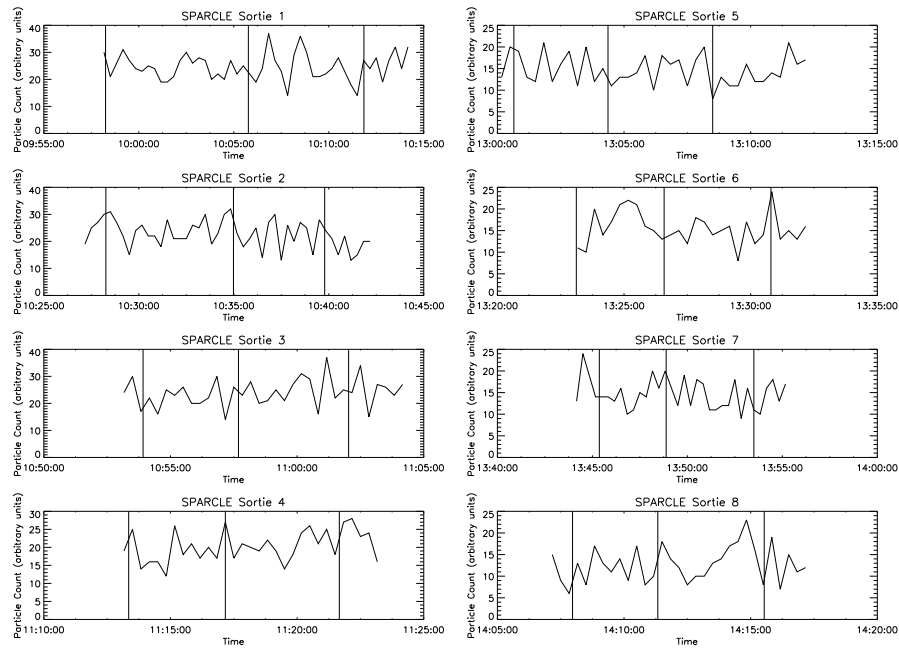


Figure 17: SPARCLE data for all sorties. Particle count axis has undefined units; the signal is proportional to particle count per cc of aerosols with diameter greater than  $0.3 \mu\text{m}$ .

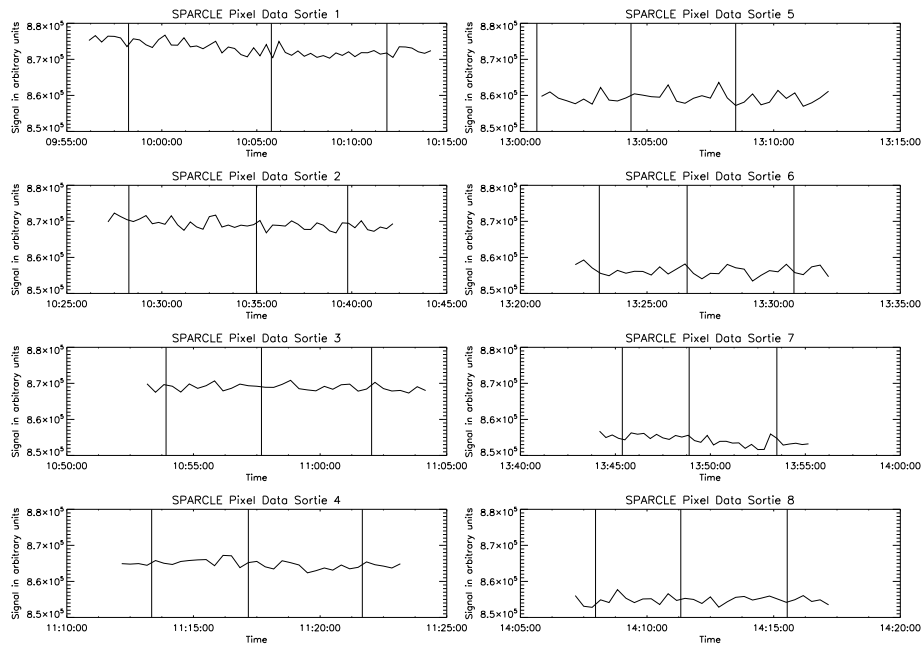


Figure 18: SPARCLE pixel data for all sorties. Vertical lines are event markers of when kerosene or tyre smoke smell was detected at inlets. The signal is proportional to particle size.

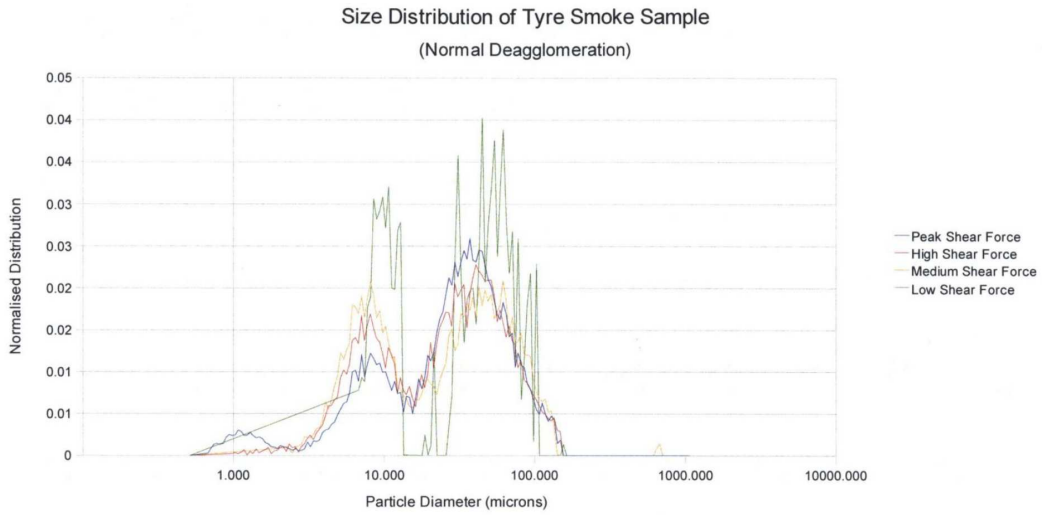


Figure 19: Size distribution of tyre and brake brushings sample (16/10/08) from undercarriage of BAE-146 displaying 3 distinct peaks at  $\sim 1.2 \mu\text{m}$ ,  $7.0 \mu\text{m}$  and  $35 \mu\text{m}$  diameters.

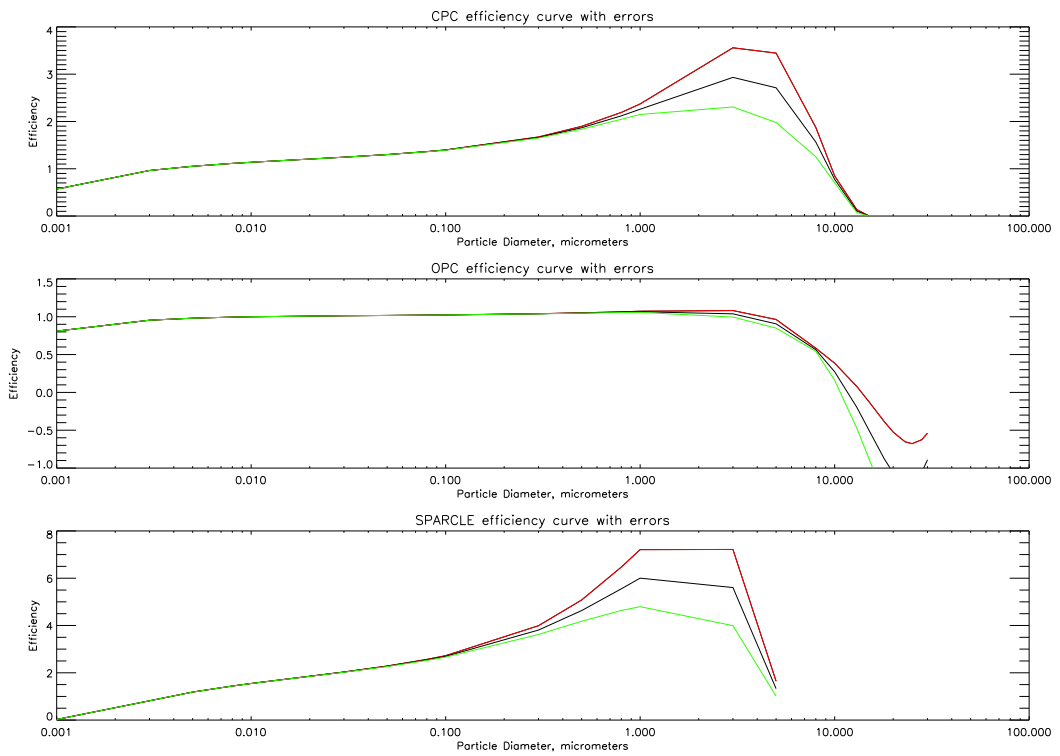


Figure 20: Efficiency curves for the instrument inlets. The black line represents the best estimate with the red and green lines corresponding to upper and lower bounds respectively. OPC and CPC are considered efficient below  $10 \mu\text{m}$  and SPARCLE below  $7 \mu\text{m}$ .